Am J Physiol Heart Circ Physiol 294: H1736–H1744, 2008.
First published February 8, 2008; doi:10.1152/ajpheart.91507.2007.

HSP27 regulates p53 transcriptional activity in doxorubicin-treated fibroblasts and cardiac H9c2 cells: p21 upregulation and G_2/M phase cell cycle arrest

C. D. Venkatakrishnan,[1] Kathy Dunsmore,[2] Hector Wong,[2] Sashwathi Roy,[3] Chandan K. Sen,[3] Altaf Wani,[4] Jay L. Zweier,[1] and Govindasamy Ilangovan[1]

[1]*Division of Cardiovascular Medicine, Department of Internal Medicine,* [3]*Department of Surgery, Davis Heart and Lung Research Institute,* [4]*Department of Radiation, The Ohio State University, Columbus; and* [2]*Division of Critical Care Medicine, Cincinnati Children's Hospital and Department of Pediatrics, University of Cincinnati College of Medicine, Cincinnati, Ohio*

Submitted 20 December 2007; accepted in final form 4 February 2008

Venkatakrishnan CD, Dunsmore K, Wong H, Roy S, Sen CK, Wani A, Zweier JL, Ilangovan G. HSP27 regulates p53 transcriptional activity in doxorubicin-treated fibroblasts and cardiac H9c2 cells: p21 upregulation and G_2/M phase cell cycle arrest. *Am J Physiol Heart Circ Physiol* 294: H1736–H1744, 2008. First published February 8, 2008; doi:10.1152/ajpheart.91507.2007.—Treatment of cancer patients with anthracyclin-based chemotherapeutic drugs induces congestive heart failure by a mechanism involving p53. However, it is not known how p53 aggravates doxorubicin (Dox)-induced toxicity in the heart. On the basis of in vitro acute toxicity assay using heat shock factor-1 (HSF-1) wild-type (HSF-$1^{+/+}$) and HSF-1-knockout (HSF-$1^{-/-}$) mouse embryonic fibroblasts and neonatal rat cardiomyocyte-derived H9c2 cells, we demonstrate a novel mechanism whereby heat shock protein 27 (HSP27) regulates transcriptional activity of p53 in Dox-treated cells. Inhibition of p53 by pifithrin-α (PFT-α) provided different levels of protection from Dox that correlate with HSP27 levels in these cells. In HSF-$1^{+/+}$ cells, PFT-α attenuated Dox-induced toxicity. However, in HSF-$1^{-/-}$ cells (which express a very low level of HSP27 compared with HSF-$1^{+/+}$ cells), there was no such attenuation, indicating an important role of HSP27 in p53-dependent cell death. On the other hand, immunoprecipitation of p53 was found to coimmunoprecipitate HSP27 and vice versa (confirmed by Western blotting and matrix-assisted laser desorption/ionization time of flight), demonstrating HSP27 binding to p53 in Dox-treated cells. Moreover, upregulation of p21 was observed in HSF-$1^{+/+}$ and H9c2 cells, indicating that HSP27 binding transactivates p53 and enhances transcription of p21 in response to Dox treatment. Further analysis with flow cytometry showed that increased expression of p21 results in G_2/M phase cell cycle arrest in Dox-treated cells. Overall, HSP27 binding to p53 attenuated the cellular toxicity by upregulating p21 and prevented cell death.

redox signaling; DNA repair; cell survival; oxidative stress

DOXORUBICIN (Dox) and its derivatives are used as chemotherapeutic drugs to treat various malignancies, such as breast cancer, in humans. The effective use of this drug is, however, limited because of its cardiotoxicity (22). Although arrhythmia is commonly observed as acute cardiotoxicity, chronic use of these drugs causes dilated cardiomyopathy and congestive heart failure among Dox-treated cancer patients (28). Thus new derivatives and improved formulations of Dox with less toxicity to the heart have been developed (22, 28). Nevertheless, cardiotoxicity remains a serious problem. Recent mechanistic studies have revealed that Dox kills cardiomyocytes and cancer cells by different mechanisms. This difference in action has rekindled interest in a thorough understanding of these mechanisms and gives hope that, by selective targeting of some of the pathways, the inevitable loss of myocytes in the heart could be avoided (22, 28).

Although cancer cell death occurs by DNA intercalation of Dox and inhibition of topoisomerase II, myocytes in the heart are lost as a result of increased oxidative stress caused by redox cycling of Dox. In both cases, apoptotic cell death has been found to occur (22). In cardiac cells, redox cycling of Dox leads to the formation of reactive oxygen species, oxidative stress, and activation of MAPK and subsequent cell death (16, 20). Different approaches, such as supplementation with various antioxidants (1), have been developed to nullify the Dox-induced oxidative stress in the heart. Also, induction of various endogenous antioxidants in the heart, such as cardiac-specific overexpression of cysteine-rich metallothionines, has been found to yield positive effects (37). We and others have established that preinduction of small heat shock proteins (HSPs), such as HSP27 (or the murine homolog HSP25), can reduce oxidative stress (10, 11, 34, 35). Small HSPs differ from larger HSPs, mainly in two ways. *1*) Because these small HSPs do not have an ATPase domain, their function does not depend on ATP. *2*) In contrast to the larger HSPs, these proteins act not only as molecular chaperonins, they are also directly involved in redox signaling, such as negative regulation of cytochrome *c* release, to prevent apoptosis (27).

Recent work in our laboratory has shown that HSP27 plays multiple roles in preventing Dox-induced toxicity (34, 35). First, we found that heat shock increased HSP27 phosphorylation by p38 MAPK and, subsequently, actin polymerization, while Dox-induced apoptosis was reduced (35). We also observed that overexpression of HSP27 increased SOD activity and protected aconitase from superoxide-induced inactivation of aconitase (12). In the present work, we report a novel finding: the transcriptional activity of p53 is regulated by HSP27. We show a novel mechanism whereby HSP27 binding to p53 increased the transcription of p21. Such an upregulation of p21 involves G_2/M cell cycle arrest, DNA repair, and cell survival. We use three different cell lines, neonatal rat cardiomyocytes derived from H9c2 cells and heat shock factor (HSF)-1 (which transcripts HSP27) wild-type (HSF-$1^{+/+}$) and HSF-1-knockout (HSF-$1^{-/-}$) mouse embryonic fibroblasts, to prove this mechanism. Since it is difficult to modulate the HSP27 level in freshly isolated adult cardiomyocytes, we

Address for reprint requests and other correspondence: G. Ilangovan, 392, BRT, The Ohio State Univ., 460 West 12th Ave., Columbus, OH 43210 (e-mail: Govindasamy.Ilangovan@osumc.edu).

The costs of publication of this article were defrayed in part by the payment of page charges. The article must therefore be hereby marked "*advertisement*" in accordance with 18 U.S.C. Section 1734 solely to indicate this fact.

chose cardiac cell lines. Cardiac H9c2 cells are from a clonal muscle cell line derived from embryonic rat hearts. Although these cells display certain features of skeletal muscle (8, 13), they retain many features of cardiac muscle, such as expression of a cardiac isoform of creatine phosphokinase, L-type Ca^{2+} channels, and the tissue-specific splicing protein smN (7, 9). In previous studies reported in the literature, this cell line was used as a model system to evaluate various characteristics of cardiomyocytes, including Dox-induced cardiotoxicity (5, 17). Also, previous studies of this cell line revealed that various HSPs can be induced by heat shock (23, 24), pharmacological induction (31, 33), or viral vector transfection (3). On the other hand, HSF-$1^{+/+}$ and HSF-$1^{-/-}$ immortalized embryonic fibroblasts have been demonstrated to be good models to study HSP effects on redox signaling (21, 29, 38).

MATERIALS AND METHODS

Chemicals and reagents. Antibodies were obtained from Stressgen, except MDM2 and the full-length p53, which were obtained from Santa Cruz Biotechnology. All other chemicals and reagents are of analytical grade, if not otherwise stated.

Cell culture. Cardiac H9c2 cells (CRL 1446, American Type Tissue Collection, Rockville, MD) were cultured as described elsewhere (34) and plated in a 150-cm^2 flask and grown at 37°C in 95% air-5% CO_2, with change of medium every 24 h. When they reached 80–90% confluency, the cells were washed with ice-cold 1× PBS (pH 7.4), trypsinized, and centrifuged at 1,500 rpm for 5 min. Cell pellets were resuspended in fresh DMEM and further passaged or appropriately treated. HSF-$1^{+/+}$ and HSF-$1^{-/-}$ cells (a kind gift from I. J. Benjamin, University of Utah) were maintained in high-glucose DMEM (without sodium pyruvate) supplemented with 10% heat-inactivated FBS, 1% penicillin-streptomycin, 1% MEM nonessential amino acid, and 500 μl of β-mercaptoethanol (GIBCO Invitrogen). When they reached 80–90% confluency, the cells were passaged into fresh medium.

Heat shock treatment. Cardiac H9c2, HSF-$1^{+/+}$, and HSF-$1^{-/-}$ cells were subjected to heat shock at 42°C for 4 h in a preheated incubator with 95% air-5% CO_2 and then incubated at 37°C for 24 h (to express HSPs after activation of HSF-1).

MTT assay. The (3,4,5-dimethylthiazol-2-yl)-2,5-diphenyltetrazolium bromide (MTT) assay was carried out as described previously (12). Cell viability is expressed relative to no drug treatment as a percentage. Cell viability in MTT assay is a measure of mitochondrial dehydrogenase activity. Viable cells convert MTT to a purple-colored insoluble component of MTT that is solubilized in MTT solvent, and the absorbance is measured at 570 nm against 690 nm as background wavelength.

Dox treatment. Dox was added directly to the medium. All three cell lines were treated with Dox for 6 h at 37°C, and toxicity was measured after 2 or 24 h. The effect of pifithrin-α (PFT-α, an inhibitor of p53) was measured by MTT assay of cell viability. First, the optimum concentration of PFT-α was obtained by a dose-dependent study. Equal numbers of cells (100 μl of 4×10^5 cells/ml) were seeded in a 96-well plate and incubated at 37°C. PFT-α (0, 0.25, 1, 5, 10, 15, and 30 μM) was added, the cells were incubated for 24 h, and viability was measured. At ≤15 μM PFT-α, no significant toxicity was observed. Thus, 15 μM was used to study the effect of PFT-α on Dox-induced toxicity. To assess the effect of PFT-α on Dox-induced toxicity, cells at 80–90% confluency were incubated with 15 μM PFT-α 30 min before addition of 0, 0.25, 0.75, 1.0, 5.0, or 10.0 μM Dox. After 6 h, Dox was withdrawn and replaced with the regular medium containing no PFT-α.

Western blot analysis. Cells were washed in ice-cold 1× PBS, trypsinized, and pelleted at 1,500 rpm for 5 min. The cells were resuspended in RIPA buffer [1× Tris-buffered saline, 1% Nonidet P-40, 0.5% sodium deoxycholate, 0.1% SDS, 0.004% sodium azide, 1× protease inhibitor (Santa Cruz Biotechnology), 1 mM phenylmethylsulfonyl fluoride, and 1 mM sodium orthovanadate] for 45 min at 4°C, and supernatants were normalized for protein concentration by the bicinchoninic acid method (Pierce). Protein (20 μg) in whole cell lysate or immunoprecipitated samples were loaded on precasted 4–12% Bis-Tris gel (Invitrogen) for electrophoresis and transferred to polyvinylidene difluoride membranes. The membranes were washed with Tris-buffered saline + Tween 20, blocked in 5% milk, and treated with the following polyclonal antibodies (1:1,000 dilution): p53 (total), p21, MDM2, Bax, Bcl-2, HSP25, and phosphorylated (Ser^{15} and Ser^{85}) HSP25. Equal loading of samples was confirmed by comparison with a GAPDH immunoblot.

Coimmunoprecipitation of HSP27 and p53. The association of p53 and HSP27 was studied by immunoprecipitation of p53 and immunoblotting of HSP27 (and vice versa) from all three cell lines using the Exacta Cruz F kit (Santa Cruz Biotechnology) according to the manufacturer's protocol. Preclearing matrix (catalog no. sc-45057; 40 μl) was added to the normalized protein samples of whole cell lysate (300 μg), which were mixed gently in a rocker at 4°C for 1 h. Then 2 μg of full-length p53 (Stressgen) or rabbit monoclonal HSP27 antibody and 500 μl of PBS were added, and the samples were incubated at 4°C in a rocker for 1 h. The beads were centrifuged and pelleted at 1,500 rpm for 5 min and washed twice with 500 μl of PBS. After the final wash, the precleared lysates were added to immunoprecipitated antibody-immunoprecipitated matrix complex beads and left overnight at 4°C once again on a rocker. Beads were pelleted at 1,500 rpm and washed three times with RIPA buffer; after the final wash, 15 μl of 4× sample loading buffer were added, and the samples were boiled at 100°C for 5 min and centrifuged at 1,500 rpm. The protein samples were electrophoresed and blotted as elaborated above. The Western blot-transferred membrane of p53 immunoprecipitates was immunoblotted for HSP27 and vice versa to confirm the coimmunoprecipitation.

Fluorescence imaging of p21. Microscopic imaging of p21 expression was carried out by staining for p21, F-actin, and nuclei (see below). Cells were grown on coverslips (BD Biosciences). At 40–50% confluency, the cells were heat shocked and then treated with Dox or directly treated with Dox (see above). After Dox treatment, cells were permeabilized in 0.2% Triton X-100 and blocked in 1% BSA-PBS for 1 h at room temperature. After addition of 100 μl of p21 monoclonal antibody (1:100 dilution in 1% BSA-PBS) and 1 h of incubation, the cells were exposed to 100 μl of secondary antibody conjugated with Alexa 456 (green fluorescence) for 45 min. For F-actin staining, the same cells were further stained with 100 μl of phalloidin-Alexa 558 (1:40 dilution in PBS-Tween, red fluorescence) for 20 min. For nuclear staining, 4,6-diamidino-2-phenylindole (1:10,000 dilution) was used. After exposure of the cells to all three stains, coverslips were mounted on the glass slides, which were sealed with Fluoromount and observed under a fluorescence microscope. Three different excitation and observation wavelengths were used to obtain images of p21, F-actin, and nuclei, and all three images were finally collated.

MALDI-TOF analyses. Mass spectral analysis, using matrix-assisted laser desorption/ionization time of flight (MALDI-TOF) was carried out for the identification of proteins in the immunoprecipitates. The unknown bands at 27 kDa were excised using a ProteomeWorks Spot Cutter (Bio-Rad), which was used to transfer the gel plugs directly to a 96-well plate. The 96-well plate was transferred to an autodigester and spotter (Proteome Works System, Perkin Elmer). The proteins were enzymatically digested, and the tryptic peptides were ZipTip purified. After ZipTip purification, the tryptic peptides were eluted from the ZipTip with 2 mg/ml cyano-4-hydroxycinnamic acid solution in 60% acetonitrile-0.2% formic acid and spotted directly onto MALDI target. The tryptic peptides on the MALDI target plate were analyzed with a MALDI-TOF spectrometer (Waters, Milford, MA). Mass spectra were acquired in the positive-ion, delayed-extraction

mode. All spectra were acquired with 20-kV accelerating voltage and checked to verify accuracy of masses for the trypsin autodigestion peptides and matrix peaks. If accuracy could not be verified, the spectra were internally mass calibrated with the protonated molecular ions $(M + H)^+$ of trypsin autodigestion peptides [mass-to-charge ratio (*m/z*) 515.33, 842.51, and 2211.10] and matrix peak (*m/z* 568.12). Data analyses were performed through the web-based MS-Fit program.

Cell cycle arrest analysis. Control and heat-shocked cardiac H9c2, HSF-1$^{+/+}$, and HSF-1$^{-/-}$ cells were treated with Dox, trypsinized, washed in ice-cold PBS, and fixed in 2.0 ml of ice-cold ethanol (75%) and left at −20°C overnight. After overnight fixation, cells were washed and resuspended in 1.0 ml of PBS. DNase-free bovine pancrease RNase (catalog no. 78020 Y, Sigma-Aldrich; 10 μl, final concentration 1 mg/ml) and then 10 μl of propidium iodide (1 mg/ml) were added to 1.0 ml of cell suspension in dark. Cell suspensions were mixed and incubated at 37°C for 30 min and analyzed by BD FACS Calibur at 617-nm emission wavelength. The DNA content-frequency histogram was analyzed using WINMDI.2.8 software and used to calculate percentage of cells in respective phases of the cell cycle.

Data analysis. Values are means ± SE. Statistical analysis was performed using Student's *t*-test and one-way ANOVA. The acceptance level of significance was $P < 0.05$.

RESULTS

Inhibition of p53-dependent Dox toxicity by PFT-α depends on HSP27 level in cardiac cells. Recently, it was reported that Dox-induced cardiotoxicity is mediated by p53 and that addition of PFT-α attenuated the cardiotoxicity (4, 19). Thus, in the first set of experiments, effects of PFT-α on Dox-induced toxicity in HSF-1$^{+/+}$, HSF-1$^{-/-}$, and H9c2 cells were evaluated. The PFT-α concentration was chosen on the basis of a dose-dependent toxicity curve constructed in the concentration range 0–30 μM. At ≤15 μM PFT-α, no significant toxicity was noted (data not shown). The cells were treated with 15 μM PFT-α 30 min before the addition of Dox, and toxicity was assessed after 24 h (see MATERIALS AND METHODS). Addition of PFT-α increased the viability of Dox-treated cardiac H9c2 and

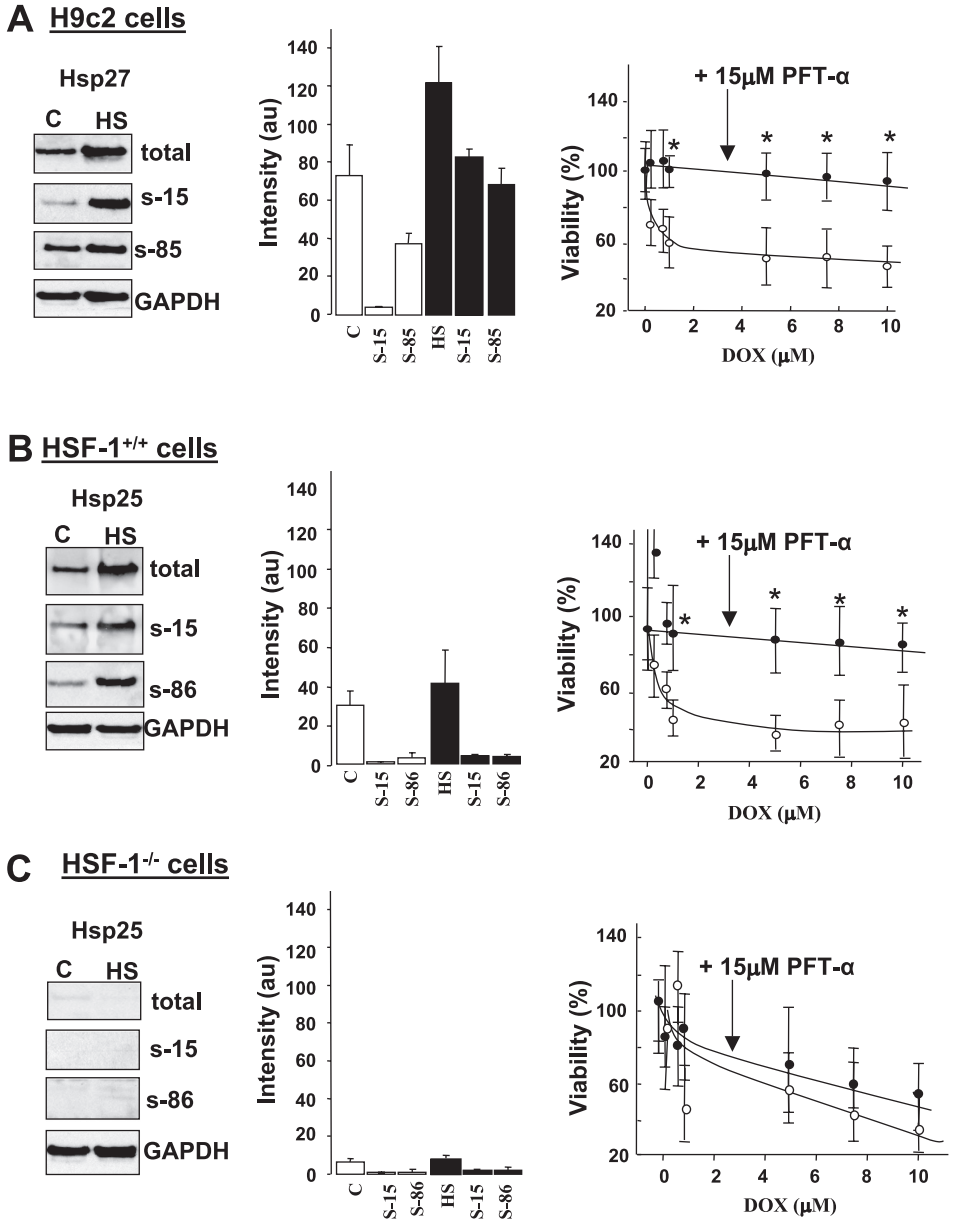

Fig. 1. Heat shock protein (HSP27) levels and protective effects of pifithrin-α (PFT-α) in doxorubicin (Dox)-treated cardiac H9c2, heat shock factor-1 (HSF-1) wild-type (HSF-1$^{+/+}$), and HSF-1-knockout (HSF-1$^{-/-}$) cells. *A*: Western blots of total HSP27 and phosphorylated (Ser^{15} and Ser^{85}) HSP27 and effect of PFT-α on Dox-induced toxicity in H9c2 cells. Heat shock (HS) at 42°C increased expression of HSP27 compared with control (C), reflecting HSF-1 activation, as shown in quantitative plots. Values [arbitrary units (au)] were plotted after normalization with respect to GAPDH as loading control. Cells were treated with 0.25–10 μM Dox for 6 h, and viability was assessed by (3,4,5-dimethylthiazol-2-yl)-2,5-diphenyltetrazolium bromide (MTT) assay 24 h later. PFT-α-treated cells were incubated with 15 μM PFT-α for 30 min before Dox treatment. *$P < 0.05$. *B*: Western blots of HSP25 and phosphorylated (Ser^{15} and Ser^{86}) HSP25 in HSF-1$^{+/+}$ fibroblasts. Other experimental conditions are described in *A*. *C*: Western blots of HSP25 and phosphorylated (Ser^{15} and Ser^{86}) HSP25 in HSF-1$^{-/-}$ fibroblasts. Other experimental conditions are described in *A*.

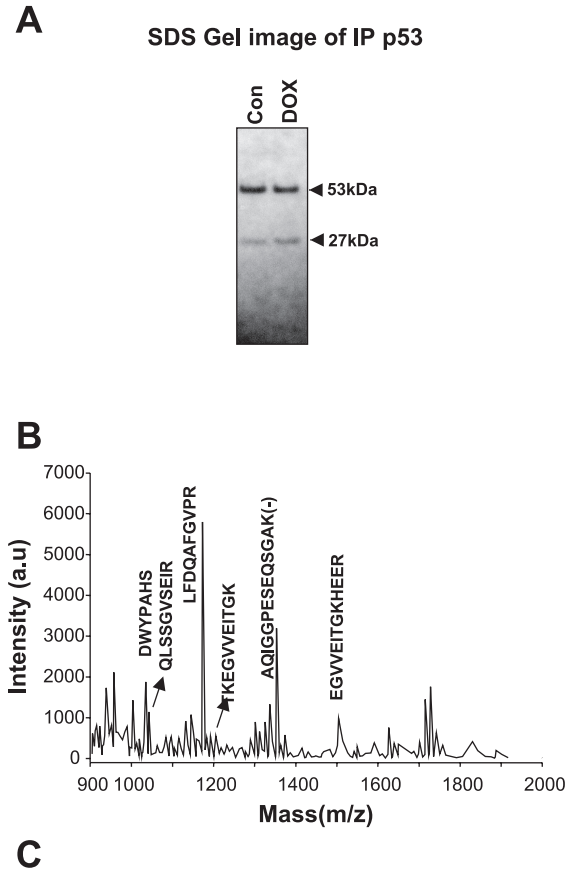

Fig. 2. Coimmunoprecipitation of HSP27 with p53. Cells were lysed, and 500 μM protein was immunoprecipitated with monoclonal p53 antibody. *A*: SDS gel image of p53 immunoprecipitates (IP) of Dox-treated cardiac H9c2 cells lysates. In addition to the p53 band at 53 kDa, another band was observed at 27 kDa. Similar bands with less intensity were observed for HSF-$1^{+/+}$ cells, but no band was observed for HSF-$1^{-/-}$ cell lysates. *B*: representative matrix-assisted laser desorption/ionization (MALDI-TOF) spectrum of 27-kDa bands dissected from the gel obtained from p53 immunoprecipitates. Peaks are labeled with corresponding peptides, identified using MS-Fit. *C*: sequence of rat HSP27. Underscored peptides are those shown by the MALDI-TOF spectrum in *B* and listed in Table 1.

HSF-$1^{+/+}$ cells (Fig. 1, *A* and *B*). However, no significant increase in viability was observed in PFT-α-treated HSF-$1^{-/-}$ cells (Fig. 1*C*). Similar results were obtained in heat-shocked H9c2, HSF-$1^{+/+}$, and HSF-$1^{-/-}$ cells (data not shown). Western blots showing the levels of total HSP27 and phosphorylated (Ser^{15} and Ser^{85}) HSP27 in H9c2 cells and phosphorylated (Ser^{15} and Ser^{86}) HSP25 in HSF-$1^{+/+}$ and HSF-$1^{-/-}$ cells are also included in Fig. 1. HSP25 is the murine homolog of HSP27 in higher organisms. In normal conditions, HSP27 and HSP25 expression is observed in H9c2 and HSF-$1^{+/+}$ cells, respectively, but, understandably, HSP25 is not detectable in HSF-$1^{-/-}$ cells. Moreover, increased levels of HSP27 in H9c2 cells and HSP25 in HSF-$1^{+/+}$ cells are observed upon heat shock, illustrating that heat shock upregulated HSP27 and HSP25 and, hence, confirming that HSF-1 is active in HSF-$1^{+/+}$ and H9c2 cells. However, no such increase in HSP25 was observed in HSF-$1^{-/-}$ cells. Overall, a direct correlation of the level of HSP27 and HSP25 expression with the increase in PFT-α-induced viability was observed in these cells. The antibodies recognize HSP25 and HSP27 in these cell lines because of their high homology of sequences (>99%; see Fig. 1 in supplemental data available in the online version of this article at the *American Journal of Physiology-Heart and Circulatory Physiology* website), and also they are functionally similar; hence, we refer to them as HSP27.

HSP27 binding with p53. In the next set of experiments, the interaction of HSP27 with p53 was determined by coimmunoprecipitation. Figure 2*A* shows the Coomassie blue-stained gel image of immunoprecipitates of p53 from control and 0.25 μM Dox-treated H9c2 cell lysates. In addition to the p53 band observed at 53 kDa, there was a distinct band at 27 kDa (Fig. 2*A*). A similar band at 25 kDa was observed for the immunoprecipitates of p53 from lysates of Dox-treated HSF-$1^{+/+}$ cells. However, the intensity of the band was weaker for HSF-$1^{+/+}$ than H9c2 cells. On the other hand, there was no such a band at 27 kDa for HSF-$1^{-/-}$ cells (data not shown).

For identification of the p53-bound 27-kDa protein in cardiac H9c2 cells, MALDI-TOF (for qualitative identification) and Western blotting (for quantitative determination) were used. These 27-kDa bands in the gels were cut, digested using trypsin, and subjected to MALDI-TOF. A representative MALDI-TOF spectrum of tryptic digest of Dox-treated cells is presented in Fig. 2*B*. MALDI-TOF data were analyzed, and the peptides were identified as described elsewhere (35). The results confirmed that these bands indeed correspond to HSP27 of the rat. In all the samples, one major peak at *m/z* 1149.63 corresponding to a singly charged peptide LFDQAFGVPR of residues 29–38 of HSP27 was observed with maximum intensity (Fig. 2*C*). In addition to this main peak, six other peptides were positively recognized (Fig. 2*B*, Table 1), as shown in Fig. 2*C*. For quantitative determination of p53-associated HSP27, HSP27 in p53 immunoprecipitates was analyzed by immunoblotting (Fig. 3, *A–C*). The association is higher in heat-shocked than in normal (non-heat-shocked) cells at all concentrations of Dox. In HSF-$1^{+/+}$ cells, bands were weaker in control cells and more intense in heat-shocked cells. However, no HSP27 was detected in immunoblots of HSF-$1^{-/-}$ cells. In another set of experiments, HSP27 was immunoprecipitated and p53 was immunoblotted under the experimental conditions described in Fig. 3, *A–C*, and the results are illustrated in Fig. 3, *D* and *E*. These results show that HSP27 binds to p53 and the magnitude of such binding depends on the HSP27 level in

Table 1. *MALDI-TOF analysis of 27-kDa band*

m/z	Comments	Peptide Sequence
1031.48		DWYPAHSR
1058.59	Pyro-Glu	QLSSGVSEIR
1075.57		QLSSGVSIR
1104.51		QDEHGYISR
1149.60		LFDQAFGVPR
1058.59		TKEGVVEITGK
1358.65		AQIGGPESEQSGAK(-)
1482.75		EGVVEITGKHEER

Matrix-assisted laser desorption/ionization time of flight was analyzed by MS-Fit. Data were fit with constraints that S and T could be phosphorylated. *m/z*, Mass-to-charge ratio.

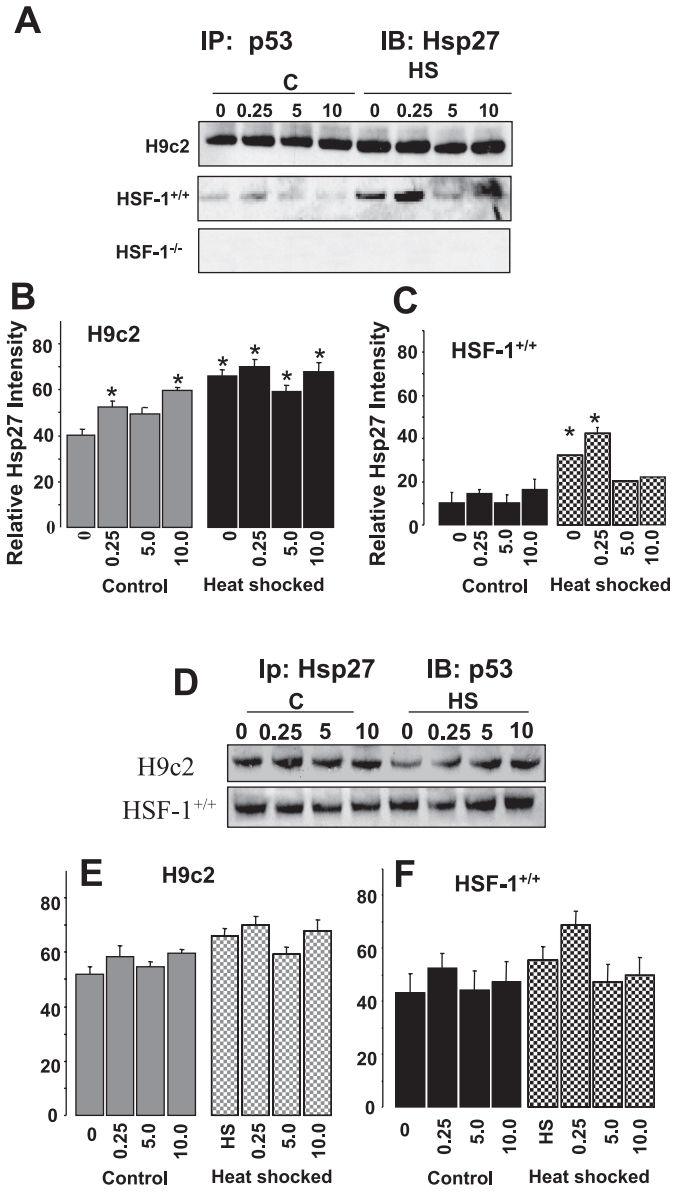

Fig. 3. Western blotting of p53 immunoprecipitates. *A*: immunoblots (IB) of HSP27 obtained from p53 immunoprecipitates of H9c2, HSF-1$^{+/+}$, and HSF$^{-/-}$ cells. Control and heat-shocked cells were treated with 0.25–10 μM Dox. After 24 h, cells were lysed and immunoprecipitated using p53 antibody and immunoblotted with HSP27. The 27-kDa protein was confirmed to be HSP27. *B* and *C*: quantitative plots of Western blot intensities for H9c2 and HSF-1$^{+/+}$ cells. *$P < 0.05$. *D*: immunoblots of p53 probed in immunoprecipitates of HSP27. *E* and *F*: quantitative plots of results from *D*. Other experimental conditions are described in *A*.

these cells. Moreover, these results also indicate that HSP27 regulates the p53-dependent cellular toxicity.

Dependence of p53 target genes on the level of HSP27. Since the magnitude of HSP27 binding to p53 is different in these cells, the levels of p53 target proteins, such as Bax, Bcl2, MDM2, and p21, were determined at two different postdrug treatment time points, 2 and 24 h (after 6 h of Dox treatment). As shown in Fig. 4*A*, at 2 h, Dox did not change the levels of Bax and Blc2 in normal and heat-shocked cells. Also there was no trace of MDM2 at 2 or 24 h. However, in normal cells, addition of 0.25 μM Dox induced p21 (~4-fold increase compared with 0 Dox; Fig. 5*A*), whereas no significant induction of p21 was observed at higher concentrations, such as 5 or 10 μM (~2-fold increase). This indicates a difference in the mechanism of cell death between low and higher Dox concentrations. It appears that, at low concentrations, cell death occurs through a p53-dependent apoptotic pathway. Indeed, in this cell line, cell death was previously reported to occur by an apoptotic pathway at low Dox concentrations and by necrosis at higher Dox concentrations (17). In heat-shocked cells, p21 increased upon treatment with 0–10 μM Dox. The p21 levels were about threefold higher than control. At 24 h, once again, no MDM2 was observed (Fig. 4*A*). Interestingly, no p21 was observed in control or heat-shocked cells (Fig. 5*A*). However, the Bcl2-to-Bax ratio was higher in heat-shocked cells. These results indicate that p21 induction occurs as an immediate response to Dox treatment and, with time, the antiapoptotic protein Bcl2 increases. As further confirmation of p21 induction, we also analyzed cell viability at 2 and 24 h in control Dox-treated cells, with the expectation of a time-dependent difference in cell viability. As expected, we observed lower viability at 2 h than at 24 h, indicating that induction of p21 results in cell cycle arrest early in the overall process (see below).

Similar analysis of p21 in HSF-1$^{+/+}$ and HSF-1$^{-/-}$ fibroblasts was carried out 2 and 24 h after drug treatment (Fig. 5). Consistently higher levels of p21, comparable to H9c2 cells, were observed at 2 h for HSF-1$^{+/+}$ fibroblasts (Fig. 5). Heat shock increased p21 expression in HSF-1$^{+/+}$ cells, as in H9c2 cells. However, p21 levels were lower at 24 h, even though PFT-α equally protected H9c2 and HSF-1$^{+/+}$ cells. This clearly shows that early induction of p21 (as shown for 2 h) is the determining factor for cell survival. On the other hand, p21 levels were low in HSF-1$^{-/-}$ cells at 2 and 24 h. Fluorescent microscopic imaging was carried out to obtain spatial confirmation of p21 in Dox-treated cardiac cells. Dox-treated control and heat-shocked cells

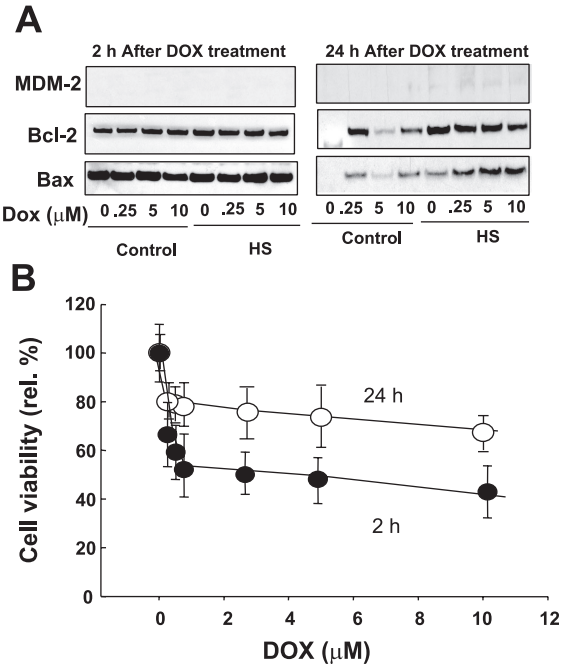

Fig. 4. MDM2, Bax, and Bcl2 expression in Dox-treated cardiac H9c2 cells. *A*: MDM2, Bax, and Bcl2 expression 2 and 24 h after treatment with 0.25–10 μM Dox. *B*: viability of normal H9c2 cells at 2 and 24 h.

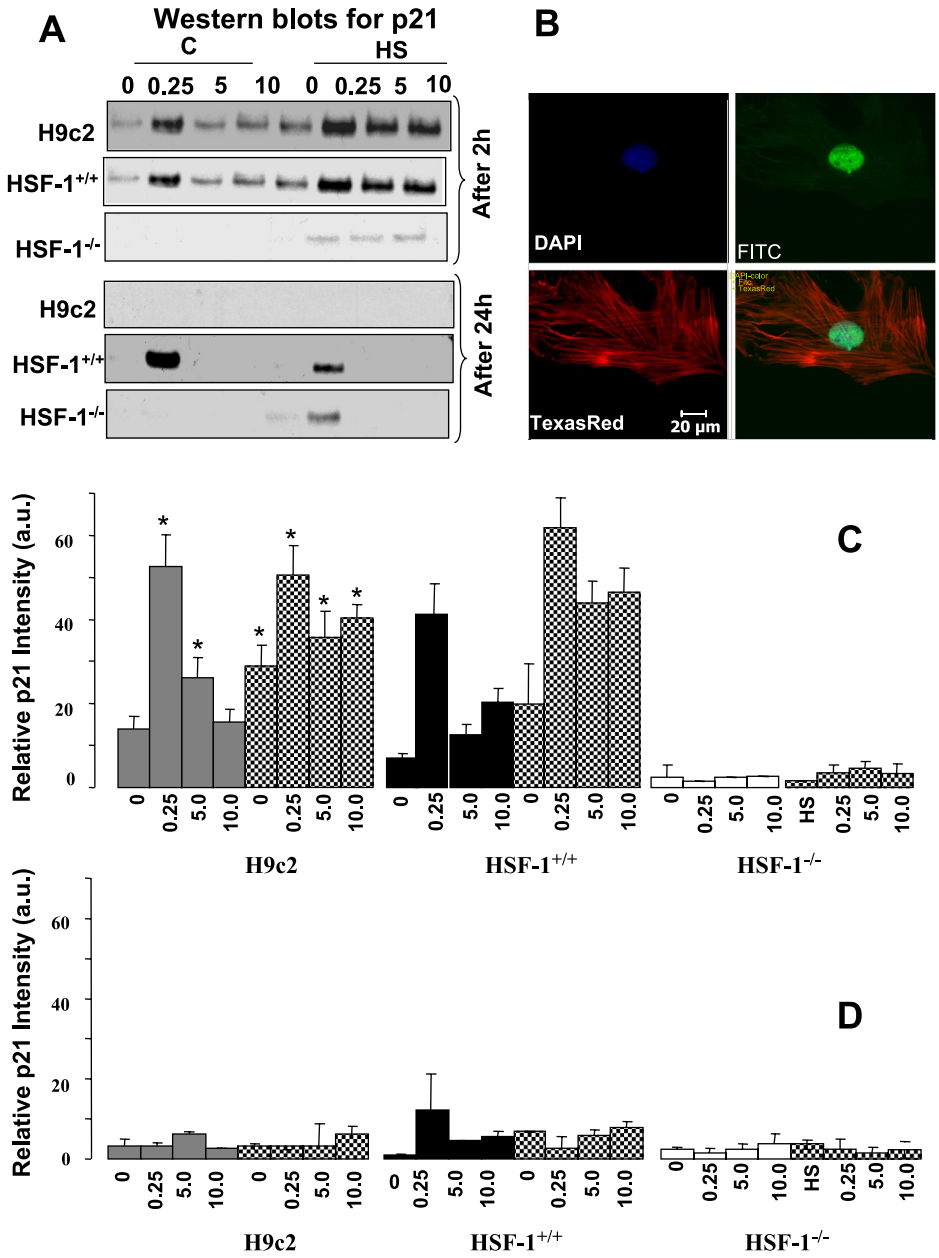

Fig. 5. Expression of p21 in normal and heat-shocked cardiac H9c2, HSF-1$^{+/+}$, HSF-1$^{-/-}$ cells. *A*: Western blots of p21 at 2 and 24 h after Dox treatment. *B*: microscopic images of cells that were double stained with Texas red-tagged actin antibody and FITC-tagged p21 antibody. Cells were treated with 0.25 μM DOX and stained 2 h later. DAPI, 4,6-diamidino-2-phenylindole. *C* and *D*: quantitative plots of Western blots in *A*. *$P < 0.05$.

were stained with FITC-tagged p21 antibody. Microscopic images of control (non-heat-shocked) H9c2 cells that were treated with 0.25 M Dox for 6 h, stained with FITC-tagged p21 antibody, and fixed 2 h after drug treatment are shown in Fig. 5*B*. The green (FITC) fluorescence was higher in Dox-treated than in control samples, confirming that Dox increased the association of HSP27 with p53 and increased the expression of p21.

HSP27-dependent G_2/M cell cycle arrest. The results summarized above show that the level of the p53 target protein p21 increased in HSP27-expressing cardiac H9c2 cells (especially in heat-shocked cells) because of increased binding of HSP27 to p53. Since the p21 protein was found to be involved in cell cycling, we next studied the effect of HSP27 level on cell cycling in Dox-treated cells. Cell distribution at different phases of cell cycling in control and heat-shocked H9c2, HSF-1$^{+/+}$, and HSF-1$^{-/-}$ cells at 0 and 5.0 μM Dox is shown in Fig. 6*A*. In control H9c2 cells (where high levels of HSP27 are expressed), Dox did not significantly change the cell population (Fig. 6). Only a very slight increase in the G_1/S phase was observed with an increase in Dox concentration. The cell population at 0 and 5 μM Dox is the same in the G_1 and G_2 phases. However, heat shock treatment of H9c2 cells (without Dox) resulted in a higher population in the G_2/M phase, indicating G_2/M phase arrest in H9c2 cells. Similar accumulation of cells at the G_2/M phase was observed in Dox-treated HSF-1$^{+/+}$ cells (Fig. 6). Interestingly, in HSF-1$^{-/-}$ cells, there is no such accumulation in the G_2/M phase, indicating that p21 induction by heat shock arrests cell cycling at the G_2/M phase in H9c2 and HSF-1$^{+/+}$ cells (Fig. 6).

DISCUSSION

The primary finding of the present work is that HSP27 regulates the transcriptional activity of p53 upon Dox-induced

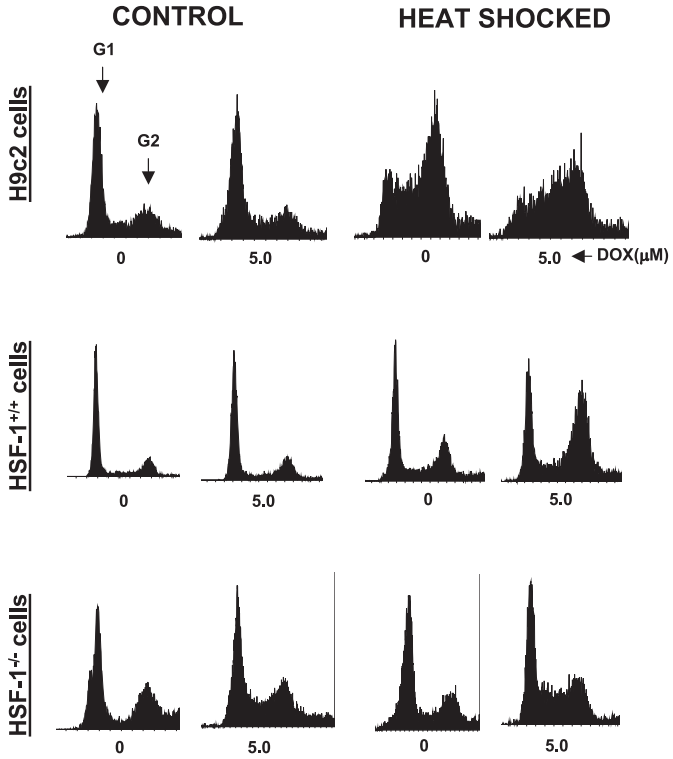

Fig. 6. Flow cytometry of cell cycle arrest. Normal and heat-shocked cells were treated with 0 and 5 μM Dox and subjected to flow cytometry. Representative histograms show distribution of cardiac H9c2, HSF-$1^{+/+}$, and HSF-$1^{-/-}$ cells treated with 0 and 5.0 μM Dox in different phases of the cell cycle.

oxidative stress in cardiac cells. Many studies have demonstrated that inhibition of p53 can protect cardiomyocytes and the heart from Dox-induced oxidative stress (19). Thus our present finding assumes importance because HSP27 may serve as an endogenous regulator of p53 transactivation in Dox-treated hearts. The results of the present study clearly demonstrate that p53-dependent cell death in Dox-treated cells is regulated by HSP27. Although many approaches have been tried to alleviate the Dox-induced cell death in the heart, methods that selectively target proapoptotic signaling have been shown to be the most efficient in preventing the loss of cardiomyocytes in the heart (18, 25). In previous studies, overexpression of HSP27 has been reported to protect cells against Dox-induced toxicity through multiple mechanisms (34, 35). Recently, we showed that the induction and phosphorylation of HSP27 by heat shock-induced MAPK increased cell viability by reducing apoptosis in Dox-treated cardiac H9c2 cells (35). In another study, we showed a direct correlation of antioxidant enzyme activity with the HSP27 level in different cell lines with different levels of HSP27 (34). In the present study, we have found that the difference in HSP27 level correlates with the difference in p53 transcriptional activity, which in turn correlates with Dox-induced toxicity.

HSPs are expressed by activation of transcription factors such as HSF-1 and HSF-2. As shown Fig. 1, heat shock yields different responses in terms of HSP27 expression in our three cell lines. Heat shock activates HSF-1, forming a homotrimer complex, which translocates into the nucleus and binds to heat shock elements to express heat shock genes and, subsequently, HSPs. However, HSF-1 knockdown has been reported to significantly reduce HSP27 expression (75% reduction compared with wild type), whereas HSP70 and HSP90 are moderately affected (34, 39). Thus, as we expected, HSP27 expression was much lower in HSF-$1^{-/-}$ cells than in cardiac H9c2 and HSF-$1^{+/+}$ cells. The present results are consistent, in that neither heat shock nor Dox could enhance HSP27 in HSF-$1^{-/-}$ cells. Thus any difference between HSF-$1^{-/-}$ cells and HSF-$1^{+/+}$ and H9c2 cells is most likely due to lack of HSP27.

Dox has been reported to transactivate p53 through upregulation of MAPK and Ser^{15} phosphorylation of p53 in response to oxidative stress (19). Such transactivation of p53 was found to increase the proapoptotic protein Bax in the heart. However, the present study has shown that the p53 inhibitor PFT-α provides differential protection against Dox toxicity in cardiac H9c2, HSF-$1^{+/+}$, and HSF-$1^{-/-}$ cells. Such protection was found to correlate with the level of HSP27 in these cells (Fig. 1). This difference in PFT-α-induced protection against Dox toxicity cannot simply be attributed to the difference in cell lines: because HSF-$1^{+/+}$ and HSF-$1^{-/-}$ are fibroblasts, they still show differential behavior, confirming that the difference in HSP27 level plays an important role in p53-dependent cell death. In previous studies, PFT-α was shown to have multiple roles in cardiac H9c2 cells and hearts (4, 19). However, the possible interplay (between p53 and HSF-1 or HSP27) has not been elucidated. The coimmunoprecipitation of p53 and HSP27 shown in the present study illustrates an association between HSP27 and p53 (Figs. 2 and 3). In cardiac H9c2 cells, where a higher level of HSP27 is expressed, the association was greater than in the other cell lines studied. In HSF-$1^{-/-}$ cells, HSP27 binding to p53 was not observed. Previous studies have reported the regulation of p53 transcriptional activity by HSP90, but nothing is known about the interaction of HSP27 with p53 (2, 32). HSP90 was found to stabilize wild-type p53

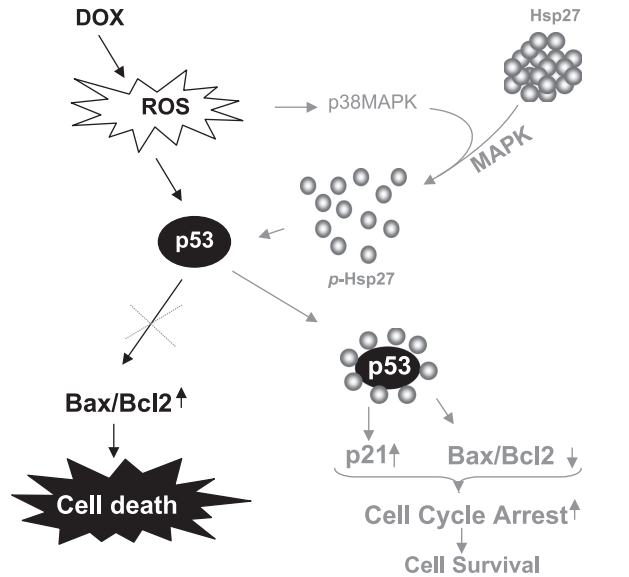

Fig. 7. Schematic illustration of proposed mechanism of p53 regulation by HSP27. Dox generates reactive oxygen species (ROS), which in turn activate p53. Activation of p53 increases transcription of Bax, which increases p53-dependent apoptosis and cell death (4). Increased expression of HSP27 (heat shock, oxidative stress, or any other mode of HSF-1 activation) and phosphorylation by MAPK result in p53 binding and increased transcription of p21. Such an increase in p21 transcription results in cell cycle arrest, DNA repair, and cell survival.

by preventing MDM2-assisted ubiquitinization in different cancer cell lines (2, 32). Such stabilization of p53 was found to increase the transcriptional activity. Recently, it was reported that HSF-1 was a powerful multifaceted modifier of carcinogenesis and that HSF-1 knockout suppressed tumor development as a result of hot-spot mutation in p53 (6). In another important study, α_B-crystallin mutation in the heart increased aggregation of HSP25 (the murine homolog of HSP27) and heart failure (30). However, to our knowledge, this is the first report of direct involvement of HSP27 as an important regulator of p53 and its transcriptional activity. However, it is not clear how HSP27 stabilizes p53 in Dox-treated cells, except that it enhances p21 transcription (see below).

Further studies of the mechanism whereby the association of HSP27 with p53 regulates cell death have shown that transcriptional activity of p53 is regulated by the bound HSP27. Dox increased the induction of p21 in H9c2 and HSF-$1^{+/+}$, but not HSF-$1^{-/-}$, cells (Fig. 5*A*). Even heat-shocked HSF-$1^{-/-}$ cells did not significantly express p21; perhaps there is no HSP27. At 2 h after Dox treatment, Bax and Bcl2 were not significantly increased (Fig. 4*A*), and no dependence on HSP27 level was observed (data not shown). However, the effect on these p53 target proteins 24 h after Dox treatment was significantly different from that 2 h after Dox treatment (Fig. 4*A*). Similarly, p21 expression decreased after 24 h. On the basis of these results, we have proposed the novel mechanism shown in Fig. 7: Dox-induced reactive oxygen species activates p53, which results in higher Bax transcriptional activity, which leads to apoptosis and cell death. However, in cells with active HSF-1 and higher HSP27 expression, as in the case of cardiac H9c2 cells, HSP27 binds with p53 and increases the transcription of p21. Such transcription of p21 leads to cell cycle arrest and DNA repair and results in cell survival. In support of the proposed mechanism, the cell cycle analysis showed increased accumulation of cells in the G_2/M phase (Fig. 6). Furthermore, the low viability 2 h after Dox treatment, compared with that 24 h after Dox treatment (Fig. 4), also supports this mechanism.

There are alternative explanations for the differential protection from Dox-induced toxicity by PFT-α. The effects of PFT-α have been shown to be very complex and multiple, and nonspecific inhibition has been reported. PFT-α has been shown to inhibit not only p53, as originally reported (14) but, also, to inhibit other transcriptional factors such as glucocorticoid receptor and HSF-1 (15). The present work showed significant attenuation of Dox-induced toxicity in H9c2 and HSF-$1^{+/+}$ cells. Interestingly, PFT-α did not attenuate Dox-induced toxicity in HSF-$1^{-/-}$ cells, indicating that p53-dependent cell death was not prevented by PFT-α. This finding supports a recent report that, instead of inhibiting p53, PFT-α inhibits one of the cofactors required for p53 activation (15). It was also found that chaperone complex is affected by PFT (26). However, our present studies have shown that the HSP90 level is not different in HSF-$1^{-/-}$ and HSF-$1^{+/+}$ cells; only the HSP27 level is reduced. Thus, PFT-α inhibits p53 in an HSP27-dependent manner.

Overall, the present work has established that HSP27 can attenuate Dox-induced toxicity by regulating the transcriptional activity of p53 and upregulating p21 (Fig. 5). Such upregulation of p21 was found to be involved in cell cycle arrest (Fig. 6), DNA repair, and cell survival (Fig. 7). However, the limitation of the present work is as follows. The Dox-induced cardiotoxicity is due to loss of cardiomyocytes triggered by oxidative stress in the heart. Cardiomyocytes are terminally differentiated, and they do not undergo cell cycling. Thus, whether HSP27 overexpression or HSF-1 knockout will protect cardiomyocytes from Dox-induced toxicity in vivo remains to be tested. If protection is observed, the mechanism of such protection may be potentially different. Independent studies with in vivo models are required to determine this mechanism.

ACKNOWLEDGMENTS

We acknowledge the help of Arun K. Tewari (Proteomics Core Facility, Davis Heart and Lung Research Institute) with the MALDI-TOF studies.

GRANTS

This study was supported by National Heart, Lung, and Blood Institute Grants R01-HL-78796 (to G. Ilangovan) and R01-HL-78087 (to C. K. Sen).

REFERENCES

1. **Berthiaume JM, Oliveira PJ, Fariss MW, Wallace KB.** Dietary vitamin E decreases doxorubicin-induced oxidative stress without preventing mitochondrial dysfunction. *Cardiovasc Toxicol* 5: 257–267, 2005.
2. **Calderwood SK, Khaleque MA, Sawyer DB, Ciocca DR.** Heat shock proteins in cancer: chaperones of tumorigenesis. *Trends Biochem Sci* 31: 164–172, 2006.
3. **Chi SH, Mestril R.** Stable expression of a human HSP70 gene in a rat myogenic cell line confers protection against endotoxin. *Am J Physiol Cell Physiol* 270: C1017–C1021, 1996.
4. **Chua CC, Liu X, Gao J, Hamdy RC, Chua BH.** Multiple actions of pifithrin-α on doxorubicin-induced apoptosis in rat myoblastic H9c2 cells. *Am J Physiol Heart Circ Physiol* 290: H2606–H2613, 2006.
5. **Corna G, Santambrogio P, Minotti G, Cairo G.** Doxorubicin paradoxically protects cardiomyocytes against iron-mediated toxicity: role of reactive oxygen species and ferritin. *J Biol Chem* 279: 13738–13745, 2004.
6. **Dai C, Whitesell L, Rogers AB, Lindquist S.** Heat shock factor 1 is a powerful multifaceted modifier of carcinogenesis. *Cell* 130: 1005–1018, 2007.
7. **Gerrelli D, Grimaldi K, Horn D, Mahadeva U, Sharpe N, Latchman DS.** The cardiac form of the tissue-specific SmN protein is identical to the brain and embryonic forms of the protein. *J Mol Cell Cardiol* 25: 321–329, 1993.
8. **Heads RJ, Latchman DS, Yellon DM.** Stable high level expression of a transfected human HSP70 gene protects a heart-derived muscle cell line against thermal stress. *J Mol Cell Cardiol* 26: 695–699, 1994.
9. **Hescheler J, Meyer R, Plant S, Krautwurst D, Rosenthal W, Schultz G.** Morphological, biochemical, and electrophysiological characterization of a clonal cell (H9c2) line from rat heart. *Circ Res* 69: 1476–1486, 1991.
10. **Hollander JM, Lin KM, Scott BT, Dillmann WH.** Overexpression of PHGPx and HSP60/10 protects against ischemia/reoxygenation injury. *Free Radic Biol Med* 35: 742–751, 2003.
11. **Hollander JM, Martin JL, Belke DD, Scott BT, Swanson E, Krishnamoorthy V, Dillmann WH.** Overexpression of wild-type heat shock protein 27 and a nonphosphorylatable heat shock protein 27 mutant protects against ischemia/reperfusion injury in a transgenic mouse model. *Circulation* 110: 3544–3552, 2004.
12. **Ilangovan G, Venkatakrishnan CD, Bratazs A, Osinbowle S, Cardounel AJ, Zweier JL, Kuppusamy P.** Heat shock-induced attenuation of hydroxyl radical generation and mitochondrial aconitase activity in cardiac H9c2 cells. *Am J Physiol Cell Physiol* 290: C313–C324, 2006.
13. **Kimes BW, Brandt BL.** Properties of a clonal muscle cell line from rat heart. *Exp Cell Res* 98: 367–381, 1976.
14. **Komarov PG, Komarova EA, Kondratov RV, Christov-Tselkov K, Coon JS, Chernov MV, Gudkov AV.** A chemical inhibitor of p53 that protects mice from the side effects of cancer therapy. *Science* 285: 1733–1737, 1999.
15. **Komarova EA, Neznanov N, Komarov PG, Chernov MV, Wang K, Gudkov AV.** p53 inhibitor pifithrin-α can suppress heat shock and glucocorticoid signaling pathways. *J Biol Chem* 278: 15465–15468, 2003.

16. **Kumar D, Lou H, Singal PK.** Oxidative stress and apoptosis in heart dysfunction. *Herz* 27: 662–668, 2002.
17. **L'Ecuyer T, Allebban Z, Thomas R, Vander Heide R.** Glutathione *S*-transferase overexpression protects against anthracycline-induced H9c2 cell death. *Am J Physiol Heart Circ Physiol* 286: H2057–H2064, 2004.
18. **Li K, Sung RY, Huang WZ, Yang M, Pong NH, Lee SM, Chan WY, Zhao H, To MY, Fok TF, Li CK, Wong YO, Ng PC.** Thrombopoietin protects against in vitro and in vivo cardiotoxicity induced by doxorubicin. *Circulation* 113: 2211–2220, 2006.
19. **Liu X, Chua CC, Gao J, Chen Z, Landy CL, Hamdy R, Chua BH.** Pifithrin-α protects against doxorubicin-induced apoptosis and acute cardiotoxicity in mice. *Am J Physiol Heart Circ Physiol* 286: H933–H939, 2004.
20. **Lou H, Danelisen I, Singal PK.** Involvement of mitogen-activated protein kinases in adriamycin-induced cardiomyopathy. *Am J Physiol Heart Circ Physiol* 288: H1925–H1930, 2005.
21. **Luft JC, Benjamin IJ, Mestril R, Dix DJ.** Heat shock factor 1-mediated thermotolerance prevents cell death and results in G_2/M cell cycle arrest. *Cell Stress Chaperones* 6: 326–336, 2001.
22. **Minotti G, Menna P, Salvatorelli E, Cairo G, Gianni L.** Anthracyclines: molecular advances and pharmacologic developments in antitumor activity and cardiotoxicity. *Pharmacol Rev* 56: 185–229, 2004.
23. **Monastyrskaya EA, Andreeva LV, Duchen MR, Manukhina EB, Malyshev IY.** Direct and cross-protective effects of heat adaptation in cultured cells. *Bull Exp Biol Med* 135: 127–129, 2003.
24. **Monastyrskaya EA, Andreeva LV, Duchen MR, Wiegant F, Bayda LA, Manukhina EB, Malyshev IY.** Adaptation to heat of cardiomyoblasts in culture protects them against heat shock: role of nitric oxide and heat shock proteins. *Biochemistry (Mosc)* 68: 816–821, 2003.
25. **Mukhopadhyay P, Batkai S, Rajesh M, Czifra N, Harvey-White J, Hasko G, Zsengeller Z, Gerard NP, Liaudet L, Kunos G, Pacher P.** Pharmacological inhibition of CB1 cannabinoid receptor protects against doxorubicin-induced cardiotoxicity. *J Am Coll Cardiol* 50: 528–536, 2007.
26. **Murphy PJ, Galigniana MD, Morishima Y, Harrell JM, Kwok RP, Ljungman M, Pratt WB.** Pifithrin-α inhibits p53 signaling after interaction of the tumor suppressor protein with HSP90 and its nuclear translocation. *J Biol Chem* 279: 30195–30201, 2004.
27. **Pandey P, Saleh A, Nakazawa A, Kumar S, Srinivasula SM, Kumar V, Weichselbaum R, Nalin C, Alnemri ES, Kufe D, Kharbanda S.** Negative regulation of cytochrome *c*-mediated oligomerization of Apaf-1 and activation of procaspase-9 by heat shock protein 90. *EMBO J* 19: 4310–4322, 2000.
28. **Peng X, Chen B, Lim CC, Sawyer DB.** The cardiotoxicology of anthracycline chemotherapeutics: translating molecular mechanism into preventative medicine. *Mol Interv* 5: 163–171, 2005.
29. **Peng ZY, Hamiel CR, Banerjee A, Wischmeyer PE, Friese RS, Wischmeyer P.** Glutamine attenuation of cell death and inducible nitric oxide synthase expression following inflammatory cytokine-induced injury is dependent on heat shock factor-1 expression. *JPEN J Parenter Enteral Nutr* 30: 400–407, 2006.
30. **Rajasekaran NS, Connell P, Christians ES, Yan LJ, Taylor RP, Orosz A, Zhang XQ, Stevenson TJ, Peshock RM, Leopold JA, Barry WH, Loscalzo J, Odelberg SJ, Benjamin IJ.** Human α_B-crystallin mutation causes oxido-reductive stress and protein aggregation cardiomyopathy in mice. *Cell* 130: 427–439, 2007.
31. **Ripley BJ, Stephanou A, Isenberg DA, Latchman DS.** Interleukin-10 activates heat-shock protein 90β gene expression. *Immunology* 97: 226–231, 1999.
32. **Sherman M, Gabai V, O'Callaghan C, Yaglom J.** Molecular chaperones regulate p53 and suppress senescence programs. *FEBS Lett* 581: 3711–3715, 2007.
33. **Stephanou A, Amin V, Isenberg DA, Akira S, Kishimoto T, Latchman DS.** Interleukin 6 activates heat-shock protein 90β gene expression. *Biochem J* 321: 103–106, 1997.
34. **Turakhia S, Venkatakrishnan CD, Dunsmore K, Wong H, Kuppusamy P, Zweier JL, Ilangovan G.** Doxorubicin-induced cardiotoxicity: direct correlation of cardiac fibroblast and H9c2 cell survival and aconitase activity with heat shock protein 27. *Am J Physiol Heart Circ Physiol* 293: H3111–H3121, 2007.
35. **Venkatakrishnan CD, Tewari AK, Moldovan L, Cardounel AJ, Zweier JL, Kuppusamy P, Ilangovan G.** Heat shock protects cardiac cells from doxorubicin-induced toxicity by activating p38 MAPK and phosphorylation of small heat shock protein 27. *Am J Physiol Heart Circ Physiol* 291: H2680–H2691, 2006.
37. **Wang GW, Klein JB, Kang YJ.** Metallothionein inhibits doxorubicin-induced mitochondrial cytochrome *c* release and caspase-3 activation in cardiomyocytes. *J Pharmacol Exp Ther* 298: 461–468, 2001.
38. **Wong HR, Dunsmore KE, Page K, Shanley TP.** Heat shock-mediated regulation of MKP-1. *Am J Physiol Cell Physiol* 289: C1152–C1158, 2005.
39. **Yan LJ, Christians ES, Liu L, Xiao X, Sohal RS, Benjamin IJ.** Mouse heat shock transcription factor 1 deficiency alters cardiac redox homeostasis and increases mitochondrial oxidative damage. *EMBO J* 21: 5164–5172, 2002.